Available online at www.sciencedirect.com
SCIENCE DIRECT
Journal of Molecular Catalysis A: Chemical 248 (2006) 32–41
JOURNAL OF MOLECULAR CATALYSIS A: CHEMICAL
www.elsevier.com/locate/molcata

Interaction of molybdenum hexacarbonyl with hydroxylated alumina thin films at high temperatures: Formation and removal of surface carbides

Y. Wang, F. Gao, W.T. Tysoe *

Department of Chemistry and Biochemistry, and Laboratory for Surface Studies, University of Wisconsin-Milwaukee, Milwaukee, WI 53211, USA

Received 13 May 2005; received in revised form 4 July 2005; accepted 6 July 2005
Available online 19 January 2006

Abstract

The chemistry of $Mo(CO)_6$ is studied on a thin hydroxylated alumina (HA) film grown in ultrahigh vacuum on a Mo(1 0 0) substrate using temperature-programmed desorption, and X-ray and Auger spectroscopies. The uptake of molybdenum on HA at ~700 K is about six times larger than on a dehydroxylated surface and this is ascribed to a combination of a higher surface area for the hydroxylated alumina film and the presence of surface hydroxyl groups. This reaction results in the formation of molybdenum carbides where the stoichiometry is close to MoC at low exposures, while it approaches Mo_2C as the exposure increases. The carbide incorporates a small amount of oxygen and measuring the Mo $3d_{5/2}$ chemical shifts suggests that the carbides are present as small particles at low $Mo(CO)_6$ exposures. With increasing exposure, the surface carbide forms a thin film. Heating the surface evolves predominantly carbon monoxide due to alumina reduction to form metallic aluminum and, at high $Mo(CO)_6$ exposures, the molybdenum diffuses into the bulk while, at lower $Mo(CO)_6$ exposures, a surface MoAl alloy is formed.

Keywords: X-ray photoelectron spectroscopy; Temperature-programmed desorption; Auger spectroscopy; Chemisorption; Molybdenum hexacarbonyl; Hydroxylated alumina thin films

1. Introduction

Molybdenum hexacarbonyl ($Mo(CO)_6$) derived catalysts are active for a number of reactions including olefin hydrogenation and metathesis [1–4]. A number of studies have been carried out on high-surface area alumina substrates, primarily using infrared spectroscopy, to understand the nature of the catalytically active species [5–12]. It has been found that subcarbonyls ($Mo(CO)_x$) derived from decarbonylation of $Mo(CO)_6$ are formed on the surface. The interaction between $Mo(CO)_6$ and alumina thin films has been studied at low temperatures in ultrahigh vacuum (UHV) [13–17], in order to mimic the realistic catalyst systems. This approach has several advantages. First, it allows model systems to be prepared that resemble the high-surface-area catalyst. Second, the alumina film is sufficiently thin that charging problems can be avoided so that it allows conventional electron- and photon-based spectroscopies to be exploited. It has been found that $Mo(CO)_6$ desorbs intact below ~250 K and reacts to form strongly bound species, which decompose at higher temperatures to desorb CO [13,15]. The strongly bound species has been identified on aluminas with various degrees of hydroxylation as an oxalate [13,15,16]. Unfortunately, only relatively small molybdenum coverages (a few percent of a monolayer) can be achieved in ultrahigh vacuum. Larger coverages can be obtained by illuminating adsorbed $Mo(CO)_6$ with ultraviolet radiation [18–20] or electrons [16]. However, the model catalysts formed using this strategy have been found to be rather inert towards olefin hydrogenation and metathesis in UHV, even with large molybdenum coverages [16]. An alternative approach is therefore undertaken by studying the interaction of $Mo(CO)_6$ with alumina thin films at high temperatures. The high-temperature interaction of $Mo(CO)_6$ with metallic aluminum [21] and dehydroxylated alumina (DA) thin films [22] has been investigated recently. It was found that a surface carbide/oxycarbide film is formed following molybdenum carbonyl reaction with both surfaces at 700 K. Heating this surface to above ~1200 K desorbs CO and forms a MoAl alloy. In order to further address the effect of the nature of the oxide substrate on the decomposition of $Mo(CO)_6$, we present in the following the results on the decomposition of $Mo(CO)_6$ at high temperatures on a thin hydroxylated alumina (HA) film grown on Mo(1 0 0).

* Corresponding author. Tel.: +1 414 229 5222; fax: +1 414 229 5036.
E-mail address: wtt@uwm.edu (W.T. Tysoe).

1381-1169/$ – see front matter © 2005 Elsevier B.V. All rights reserved.
doi:10.1016/j.molcata.2005.07.051

2. Experimental

Temperature-programmed desorption (TPD) data and X-ray photoelectron (XPS) and Auger spectra were collected in ultrahigh vacuum chambers operating at base pressures of $\sim 2 \times 10^{-10}$ Torr or lower that have been described in detail elsewhere [21]. Briefly, TPD data are detected using a Dycor quadrupole mass spectrometer placed in line of sight of the sample. Auger spectra are collected using an electron beam energy of 3 keV and the first-derivative spectrum obtained by numerical differentiation [23]. XPS data were collected using a Specs X-ray source and double-pass cylindrical mirror analyzer with an Mg Kα X-ray power of 250 W and a pass energy of 50 eV [21].

The Mo(1 0 0) substrate was cleaned using a standard procedure, which consisted of argon ion bombardment (2 kV, 1 μA/cm^2) and any residual contaminants were removed by briefly heating to 2000 K in vacuo. The resulting Auger spectrum showed no contaminants. A hydroxylated alumina thin film is formed by evaporating an aluminum film onto Mo(1 0 0) [24]. The aluminum is oxidized at ∼650 K by water vapor from a capillary doser at a background chamber pressure of $\sim 1 \times 10^{-8}$ Torr, leading to a pressure at the sample of $\sim 2 \times 10^{-6}$ Torr using an enhancement factor of ∼200 determined previously [23]. This process is repeated until the alumina film is sufficiently thick that no substrate molybdenum signals are detected using Auger or XPS. To ensure complete oxidation, only a very thin aluminum film is deposited during each deposition–oxidation cycle.

Molybdenum hexacarbonyl (Aldrich, 99%) was transferred to a glass vial, connected to the gas-handling line of the chamber and purified by repeated freeze-pump-thaw cycles, followed by distillation, and its purity was monitored using mass and infrared spectroscopies. This was also dosed onto the surface via a capillary doser to minimize background contamination. The exposures in Langmuirs ($1\,L = 1 \times 10^{-6}$ Torr s) are corrected using the same enhancement factor of 200 [23].

3. Results

Fig. 1(a) shows the Auger spectra of $Mo(CO)_6$ adsorbed on hydroxylated alumina at 700 K as a function of exposure, where the exposures are marked adjacent to the corresponding spectrum. The spectrum of hydroxylated alumina prior to carbonyl adsorption is also plotted for comparison. This reveals that the peak-to-peak intensities of the molybdenum (119, 160, 186 and 221 eV kinetic energies) and carbon KLL transitions (271 eV KE) increase with $Mo(CO)_6$ exposure, while the aluminum (53 eV KE, Al^{3+}) and oxygen (510 eV KE) features decrease. Note that the clear break to high kinetic energies of the 53 eV aluminum Auger feature (marked with an arrow) implies complete oxidation of aluminum [25]. The characteristic shape of the carbon KLL Auger feature indicates the presence of carbide. Note that the oxidation state of deposited molybdenum does not vary with increasing $Mo(CO)_6$ exposures at 700 K, indicated by the constant kinetic energies of the molybdenum transitions [21].

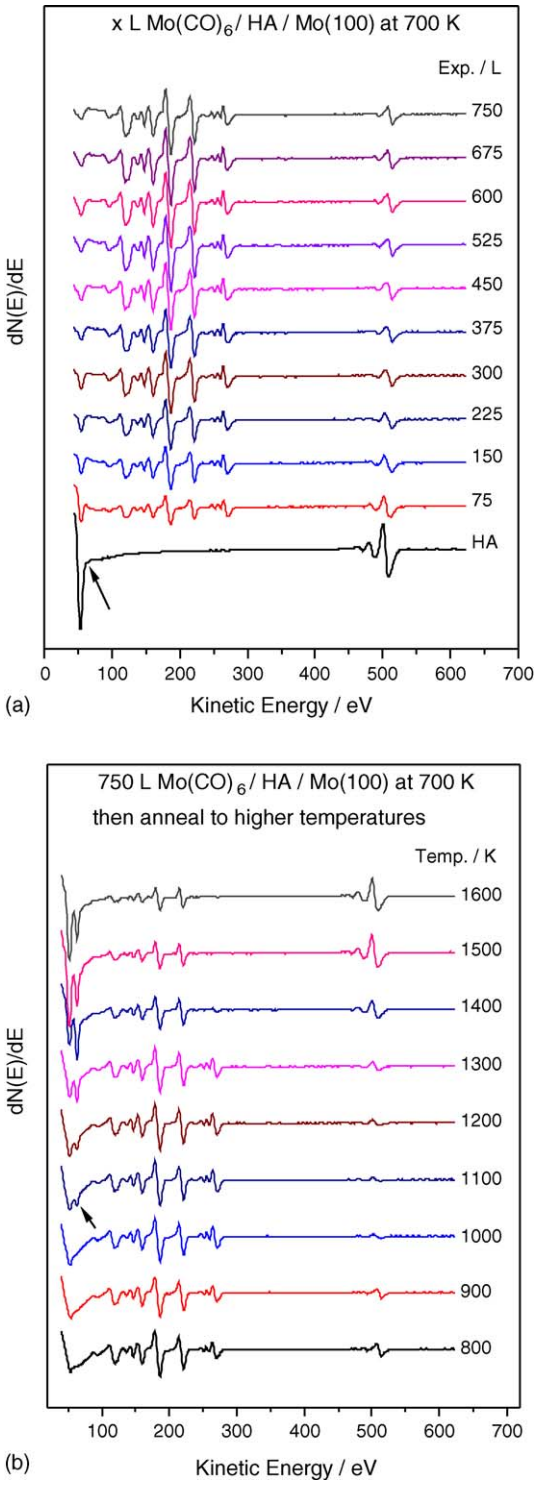

Fig. 1. Auger spectra of (a) $Mo(CO)_6$ adsorbed on hydroxylated alumina at 700 K as a function of exposure, where exposures are marked adjacent to the corresponding spectrum and (b) the effect of heating a surface exposed to 750 L of $Mo(CO)_6$ at 700 K to various temperatures, where annealing temperatures are marked adjacent to the corresponding spectrum.

Fig. 1(b) displays the results of annealing the sample to higher temperatures. Note that, in contrast to the behavior on dehydroxylated alumina [22] where alumina reduction was found to occur at temperatures higher than 1000 K, heating only to 800 K causes drastic changes. First, the intensity of aluminum Auger feature increases suggesting diffusion of molybdenum from the surface to the bulk, since no Mo desorption is observed using temperature-programmed desorption (data not shown). Second, the clear break to high energies of the aluminum Auger peak disappears suggesting alumina reduction [25]. Note that control experiments by annealing hydroxylated alumina alone to higher temperatures does not result in such changes; alumina reduction is induced by the deposited film. On further heating to 1100 K (Fig. 1(b)), a clear Al^0 feature appears at ~66 eV and is indicated by an arrow. This feature intensifies on heating to 1400 K, but decreases in intensity at higher temperatures. The carbon signal attenuates substantially at 1400 K, and by 1500 K it has disappeared completely. The oxygen signal intensity decreases substantially on heating from 800 to 1100 K, and increases again at higher temperatures. Note that during $Mo(CO)_6$ exposure and annealing, the kinetic energies of the molybdenum Auger transitions do not vary.

It has been demonstrated previously that the deposited molybdenum carbide films contain a small amount of oxygen following reaction with metallic aluminum [21] and dehydroxylated alumina [22] so that, instead of pure MoC_x, an oxycarbide MoC_xO_y is formed on the surface. In those cases, the energies of the molybdenum Auger transitions were also found not to vary [26], indicating that the oxygen content of the carbide phase is rather low. By measuring the Al^{3+}/O ratio of the surface before and after $Mo(CO)_6$ deposition at 700 K (Fig. 1), it is also found that the ratio does not vary significantly, further indicating that the oxygen content of the carbide phase is small. However, the molybdenum oxidation is more sensitive to the peak-to-peak intensity ratios of the molybdenum Auger transitions [21,27]. For pure Mo(1 0 0), the ratio $I_{119\,eV}/I_{186\,eV} = 0.19$, $I_{160\,eV}/I_{186\,eV} = 0.37$, and $I_{221\,eV}/I_{186\,eV} = 0.88$. The first two ratios are expected to increase and the latter to decrease on molybdenum oxidation. These ratios are plotted versus $Mo(CO)_6$ exposure (Fig. 2(a)), and as a function of annealing temperature (Fig. 2(b)). The data of Fig. 2(a) show that $Mo(CO)_6$ reaction with hydroxylated alumina also leads to slightly oxidized molybdenum, similar to what was found previously for films grown on aluminum and dehydroxylated alumina [21,22]. Note that the oxidation state of Mo does not vary with increasing $Mo(CO)_6$ exposures. The data of Fig. 2(b) indicate that annealing the sample causes a gradual reduction of Mo and, at 1600 K, it is almost metallic.

The $C_{271\,eV}/Mo_{186\,eV}$ Auger peak-to-peak ratios are plotted in Fig. 3(a) as a function of $Mo(CO)_6$ exposure and in Fig. 3(b) as a function of annealing temperature. These are also displayed as C/Mo stoichiometries using literature Auger sensitivity factors [28]. At low $Mo(CO)_6$ exposures (Fig. 3(a)), the C/Mo ratio is approximately unity indicating the initial film stoichiometrically resembles MoC. The ratio decreases rapidly up to an exposure of ~200 L and more slowly thereafter. This suggests that the carbide formed at high $Mo(CO)_6$ exposures becomes

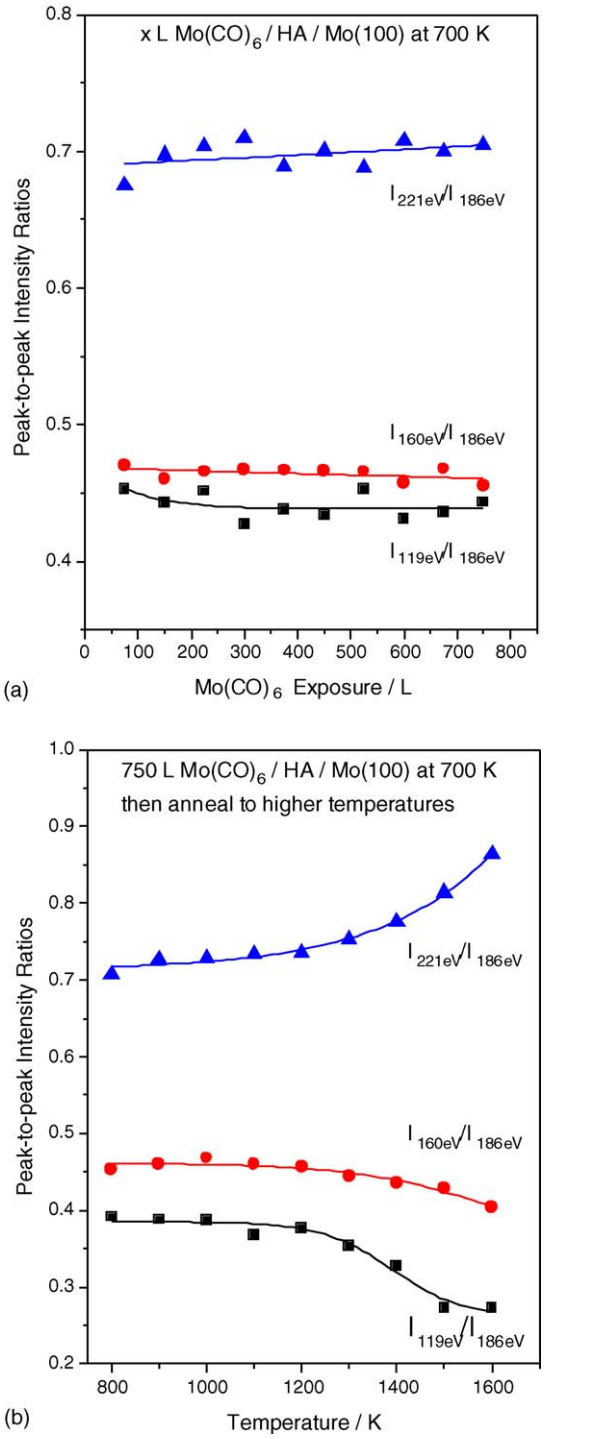

Fig. 2. Plot of the Auger peak-to-peak intensity ratios $I_{221\,eV}/I_{186\,eV}$ (▲), $I_{160\,eV}/I_{186\,eV}$ (●) and $I_{119\,eV}/I_{186\,eV}$ (■) for the deposition of $Mo(CO)_6$ on hydroxylated alumina at (a) 700 K as a function of $Mo(CO)_6$ exposure and (b) as a function of annealing temperature.

stoichiometrically closer to Mo_2C (C/Mo ~ 0.5), and a similar behavior was found when reacting $Mo(CO)_6$ with metallic aluminum [22] and dehydroxylated alumina [22]. Note, however, the exact carbide phases formed on the surface cannot be derived based on the above atomic ratio analysis. It should be mentioned that the deposited carbide film also incorporates a tiny amount

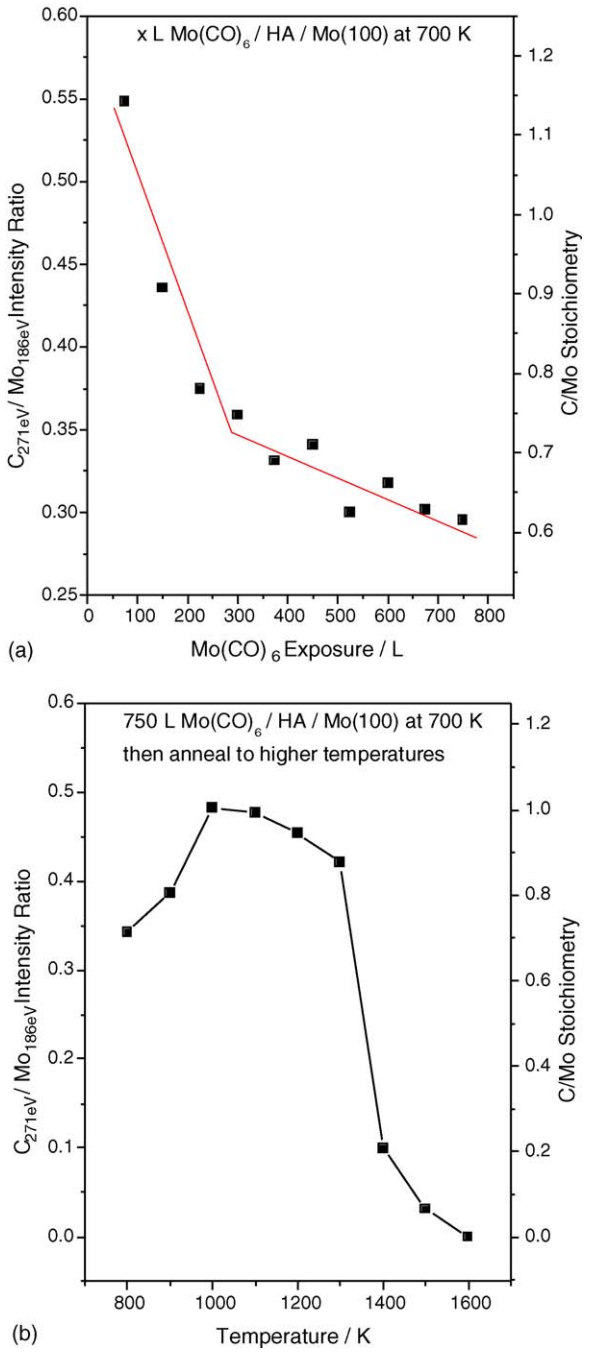

Fig. 3. Plot of the $C_{271\,eV}/Mo_{186\,eV}$ peak-to-peak Auger ratio, (a) for $Mo(CO)_6$ adsorbed on hydroxylated alumina at 700 K as a function of exposure and (b) as a function of annealing temperature after and exposure of 750 L at 700 K.

of oxygen as indicated in Fig. 2. Annealing the sample to 1000 K causes carbon diffusion to the near-surface region indicated by the C/Mo ratio increase (Fig. 3(b)). Note that carbon is still carbidic during annealing, as confirmed by the presence of a carbidic Auger lineshape (Fig. 1(b)). The C/Mo ratio decreases slowly from 1000 to 1300 K, and drastically above 1300 K.

The 28 amu (CO), 32 amu (O_2), 44 amu (CO_2) and 18 amu (H_2O) temperature-programmed desorption spectra collected at a heating rate of 15 K/s are displayed in Fig. 4 following $Mo(CO)_6$ exposures of 75 L (Fig. 4(a)), 300 L (Fig. 4(b)) and 750 L (Fig. 4(c)) at 700 K. CO has two desorption states at ~1130 and ~1330 K. Following a 75 L $Mo(CO)_6$ exposure, the intensities of these two states are comparable, while at larger exposures, the ~1130 K feature becomes substantially larger than that at ~1330 K. Recent studies using ^{18}O-labeled alumina have shown that the low-temperature state correlates with the decomposition of the initially formed oxycarbide and alumina reduction by carbidic carbon, while the high-temperature state is due exclusively to alumina reduction [22]. No CO_2 (44 amu) desorption is detected following a 75 L $Mo(CO)_6$ exposure, but a broad feature appears between 800 and 1300 K at higher exposures. Water (18 amu) desorption is detected below 1300 K in a broad feature, which decreases to zero between 1200 and 1300 K due to a gradual dehydration of hydroxylated alumina. Note that this enhanced desorption extends below 700 K, while the spectra are only displayed above this temperature. It should be mentioned that, in principle, water could originate both from surface and subsurface hydroxyl groups. It appears from the 18 amu desorption profiles plotted in Fig. 4 that the water yield decreases with increasing $Mo(CO)_6$ exposures. In order to verify this point, water desorption yield was measured from the integrated area between 700 and 1300 K and it is found that the amount of water desorbing from the surface indeed decreases with increasing $Mo(CO)_6$ exposure suggesting that hydroxyl groups are removed by reaction with $Mo(CO)_6$ and this will be discussed in greater detail below. Finally, no O_2 desorption is detected at all exposures.

The corresponding narrow scan X-ray photoelectron spectra are plotted in Fig. 5 as a function of $Mo(CO)_6$ exposure. Fig. 5(a) shows the Mo 3d region where, at $Mo(CO)_6$ exposures below 100 L, a Mo $3d_{5/2}$ binding energy of 228.2 eV (0.8 eV higher than the clean Mo(1 0 0) substrate) is found. This decreases to 227.8 eV following a $Mo(CO)_6$ exposure of 200 L, and shifts further to 227.4 eV for exposures of 400 and 700 L. Fig. 5(b) displays the corresponding Al 2p region. For $Mo(CO)_6$ exposures below 100 L, an Al 2p binding energy of 75.4 eV is found (identical to that for clean hydroxylated alumina), but shifts to 75.0 eV at 200 L, and moves even lower, to 74.5 eV, for $Mo(CO)_6$ exposures of 400 L and greater. Fig. 5(c) plots the corresponding C 1s region where, for exposures from 20 to 100 L, the binding energy decreases slightly from 284.3 to 283.7 eV. A relatively large shift to 282.9 eV is found following a 200 L $Mo(CO)_6$ exposure, finally reaching 282.5 eV at higher exposures. An O 1s binding energy of 532.5 eV is found at exposures of 20 and 50 L (Fig. 5(d); identical to that for clean, hydroxylated alumina), which decreases to 532.3 eV at 100 L, 531.8 eV at 200 L, and 531.2 eV binding energy at 400 and 700 L $Mo(CO)_6$ exposures.

The Mo $3d_{5/2}$ chemical shifts (compared to the corresponding Mo(1 0 0) substrate feature at 227.4 eV) and integrated signal intensities are plotted as a function of $Mo(CO)_6$ exposure in Fig. 6. It is found that, for $Mo(CO)_6$ exposures below 100 L, the signal intensity grows linearly and becomes constant at exposures above 400 L.

The narrow scan XP spectra collected after heating a surface following a 700 L $Mo(CO)_6$ exposure at 700 K are displayed in Fig. 7. The Mo $3d_{5/2}$ peak position remains constant at

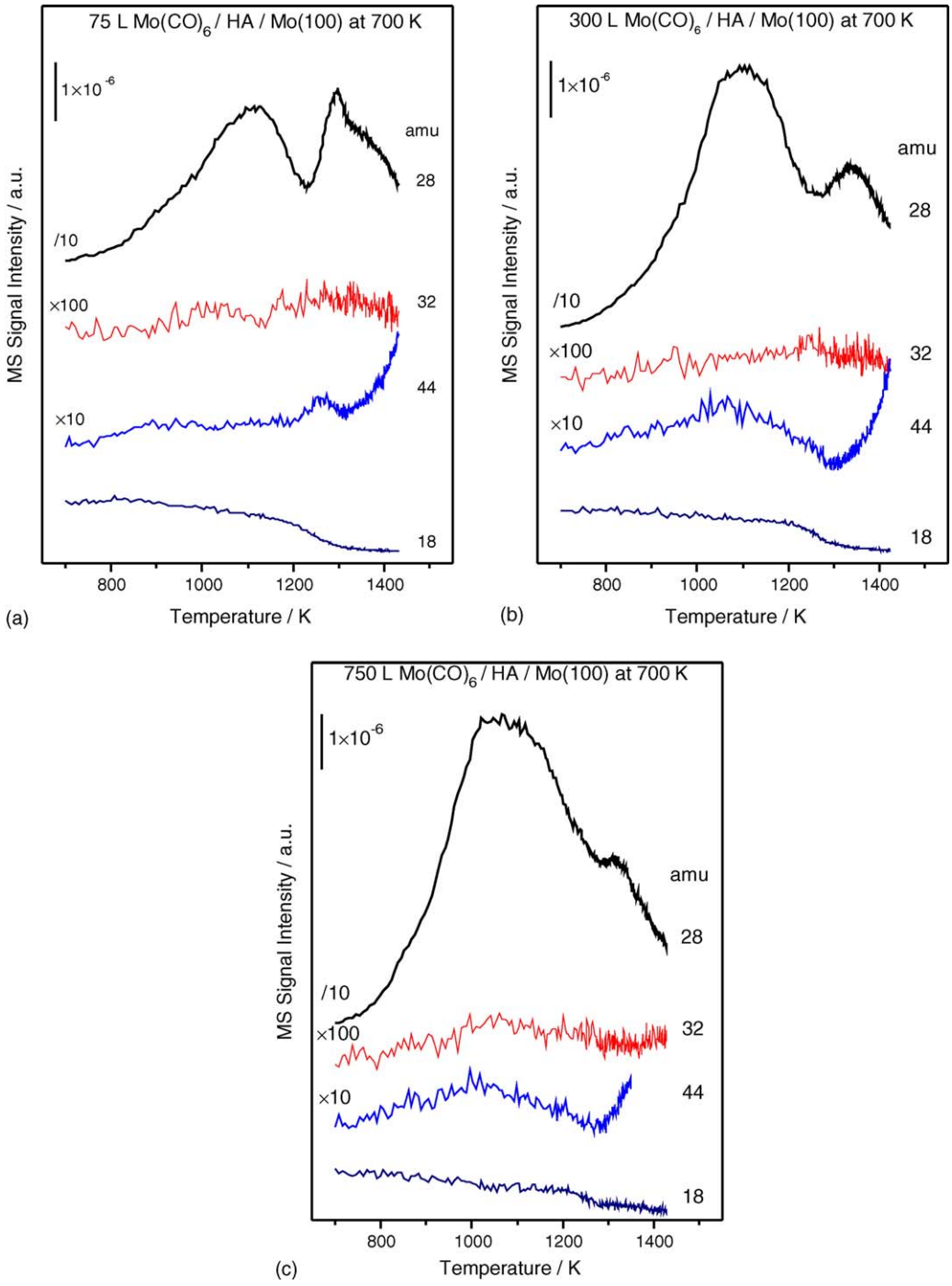

Fig. 4. The 28 amu (CO), 32 amu (O_2), 44 amu (CO_2) and 18 amu (H_2O) temperature-programmed desorption spectra collected at a heating rate of 15 K/s for $Mo(CO)_6$ exposures of (a) 75 L, (b) 300 L and (c) 300 L of $Mo(CO)_6$ at 700 K on hydroxylated alumina.

~227.3 eV on heating to between 700 and 1000 K (Fig. 7(a)). However, the spectrum broadens and shifts to 228.0 eV on heating to 1100 K, eventually shifting to 228.8 eV and decreasing in intensity on heating to 1200 K and above. The Al 2p feature (Fig. 7(b)) remains constant at ~74.5 eV on heating from 700 to 1000 K, while drastic changes occur above 1000 K where the binding energy increases to 76.6 eV at temperatures of 1200 K and higher. Fig. 7(c) displays the C 1s region where, between 700 and 1000 K, a C 1s feature is observed at 282.5 eV, which shifts to 283 eV at 1100 K and further to 284.1 eV at 1200 K. Above 1300 K, the signal intensity decreases substantially, consistent with Auger data shown in Fig. 1(b), and almost disappears at 1400 K. Fig. 7(d) shows the corresponding O 1s region, where the binding energy of the O 1s feature remains relatively constant at 531.3 eV between 700 and 1000 K and again drastic changes occur on heating to 1100 K, where an O 1s binding energy of 532.5 eV is found. Additional shifts are noted at higher temperatures so that at 1400 K, an O 1s binding energy of 533.6 eV is found. It should be mentioned that the C/Mo ratio of the film formed at 700 K and following annealing are also calculated

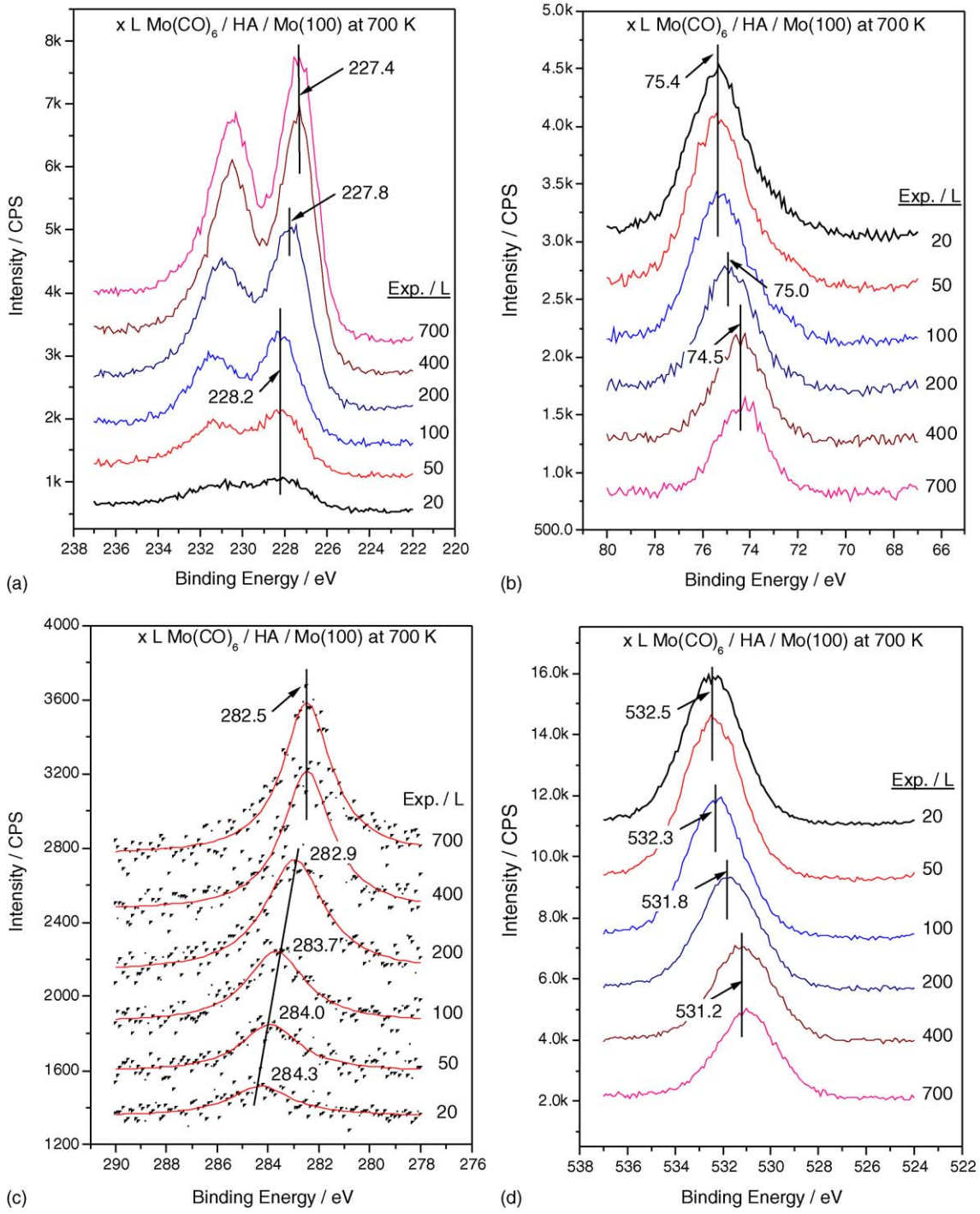

Fig. 5. Narrow scan Mg Kα X-ray photoelectron spectra of the (a) Mo 3d, (b) Al 2p, (c) C 1s and (d) O 1s regions as a function of $Mo(CO)_6$ exposure on hydroxylated alumina at 700 K, where exposures are displayed adjacent to the corresponding spectrum.

using XPS data where it is found that these values are close to those obtained using Auger analysis (Fig. 3) with uncertainties within 10%, emphasizing the consistency of these two methods.

The uptake of $Mo(CO)_6$ on alumina is monitored from the Auger data in Fig. 1 and the resulting Mo/Al ratio is plotted versus $Mo(CO)_6$ exposure in Fig. 8 (▲) and is compared with data for dehydroxylated alumina (■) [22], where the reactive sticking coefficient on $Mo(CO)_6$ on hydroxylated alumina is ∼6 times larger than on dehydroxylated alumina. TPD data shown in Fig. 4 suggest that this effect is related to the presence of surface hydroxyl groups where the amount of H_2O desorbing from the surface decreases with increasing $Mo(CO)_6$ exposure. In order to further address this issue, a dehydroxylated alumina sample was exposed to 1×10^{-6} Torr of H_2O for 10 min at 700 K to graft –OH groups onto the surface. Subsequent temperature-programmed desorption experiments (data not shown) revealed that water desorbed between 700 and 1300 K, similar to that shown in Fig. 4, indicating that surface hydroxyl groups are

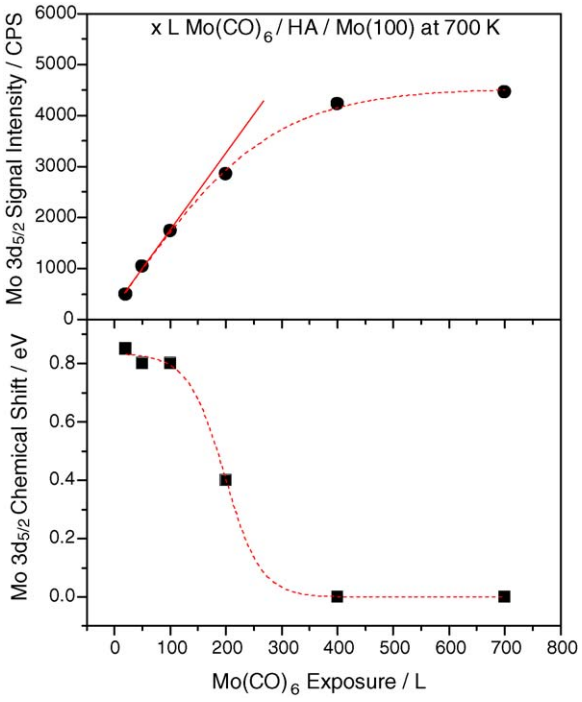

Fig. 6. Mo $3d_{5/2}$ chemical shift and signal intensity as a function of $Mo(CO)_6$ exposure on hydroxylated alumina at 700 K.

formed on the surface following this treatment. The resulting $Mo(CO)_6$ uptake at 700 K on this surface is also displayed in Fig. 8 (◯), and is identical to that on the original dehydroxylated surface. This immediately indicates that the presence of surface hydroxyl groups is not responsible for the enhanced uptake on the hydroxylated sample. This, however, will be discussed in greater detail below. It should also be pointed out that ex situ AFM measurements (not shown) have revealed that the HA surface is rougher than the DA. This may be another reason that the reactive sticking probability of $Mo(CO)_6$ on HA is larger than on DA.

It is found that heating a surface exposed to $Mo(CO)_6$ at 700 K to higher temperature causes a decrease in the amount of molybdenum detected (Figs. 1(b) and 7(a)) and an increase in binding energy (Fig. 7(a)). In contrast, the exact opposite effect is found on dehydroxylated alumina [22]. However, due to the higher reactive sticking coefficient on hydroxylated alumina than on dehydroxylated alumina, larger molybdenum coverages are attained in the latter case than the former. Hydroxylated alumina was exposed to only 50 L of $Mo(CO)_6$ to yield lower molybdenum coverages and the resulting Mo $3d_{5/2}$ spectrum is displayed in Fig. 9, as a function of annealing temperature. Now the molybdenum signal intensity increases, and its binding energy decreases similar to the behavior on dehydroxylated alumina [22].

4. Discussion

4.1. Nature of the film deposited at 700 K

The Al 2p (75.4 eV; Fig. 5(b)) and O 1s (532.5 eV; Fig. 5(d)) binding energies for HA are slightly higher than the corresponding values for dehydroxylated alumina (74.6 eV for Al 2p and 531.6 eV for O 1s [21]) consistent with the presence of surface –OH groups [29,30], in agreement with the TPD results displayed in Fig. 4, where water desorption is found below 1300 K. These binding energies shift to those found on DA [21] following large $Mo(CO)_6$ exposures (Fig. 5) suggesting that the surface hydroxyls are removed by reaction with $Mo(CO)_6$ at 700 K, also consistent with TPD results shown in Fig. 4. The nature of the initial reaction of surface hydroxyl groups with $Mo(CO)_6$ is not clear. One possibility is that hydroxyl groups are replaced by Mo species so that an Al–Mo bond is formed. On the other hand, it is also possible that surface –O–Mo bonds can form with the removal of H atoms.

A similar film composition is found on HA as on DA where a film stoichiometrically close to MoC is formed initially, but evolves into a film with a stoichiometry close to Mo_2C as the $Mo(CO)_6$ exposure increases (Fig. 3(a)). Similar to the behavior found on dehydroxylated alumina, some oxygen is incorporated into the film (Fig. 2). However, in contrast to the behavior on aluminum and DA, some carbon oxidation occurs, especially at low $Mo(CO)_6$ exposures, since the C 1s binding energy ~284.3 eV (Fig. 5(c)) is much higher than found for $Mo(CO)_6$ reaction with aluminum and DA (where the C 1s BE was 282.6 eV [21]). This is presumably due to participation of the –OH groups. Note that a similar C 1s binding energy increase was observed during the oxidation of Mo_2C [31].

A Mo $3d_{5/2}$ binding energy of 228.2 eV is found for low $Mo(CO)_6$ exposures (Figs. 5(a) and 9), 0.8 eV higher than the clean Mo(1 0 0) substrate, which may be due to molybdenum carburization, oxidation, or particle size effects [21]. Molybdenum carburization results in only small Mo 3d BE increases (typically less than 0.2 eV) [32,33]. It has been demonstrated that oxidation causes a Mo binding energy increase; however, since only a small amount of oxygen incorporates into the film formed here, no Mo chemical shift due to oxidation is expected [34,35]. Note that the oxidation state of molybdenum does not vary with increasing $Mo(CO)_6$ exposure (Fig. 2(a)). The primary origin of the relatively large binding energy increase is a particle size effect, where a decrease in particle size causes a binding energy increase when small metallic particles are deposited onto insulating substrates (alumina in this case), due to final state effects [36–39]. The data of Fig. 5(a) reveal that, at high $Mo(CO)_6$ exposures (400 and 700 L), the Mo $3d_{5/2}$ binding energy is identical to that of the Mo(1 0 0) substrate suggesting that the particle size effects are indeed responsible for the chemical shift at lower exposures. This also emphasizes that carbon and oxygen incorporation into the deposited film does not necessarily induce a Mo chemical shift. Wertheim et al. [38,39] proposed a cluster-charge model to make a simple and material-independent prediction of the size dependence of the chemical shift, which, for a free spherical cluster of radius r, is proportional to $e^2/2r$. Applying this model to the chemical shift data plotted in Fig. 6, for $Mo(CO)_6$ exposures below 100 L, the particle sizes are rather small and increase at a $Mo(CO)_6$ exposure of 200 L. For $Mo(CO)_6$ exposures of 400 L and greater, where the Mo $3d_{5/2}$ BE returns to that of clean Mo(1 0 0), this indicates that the particles become large or that a thin molybdenum carbide film is formed. Note

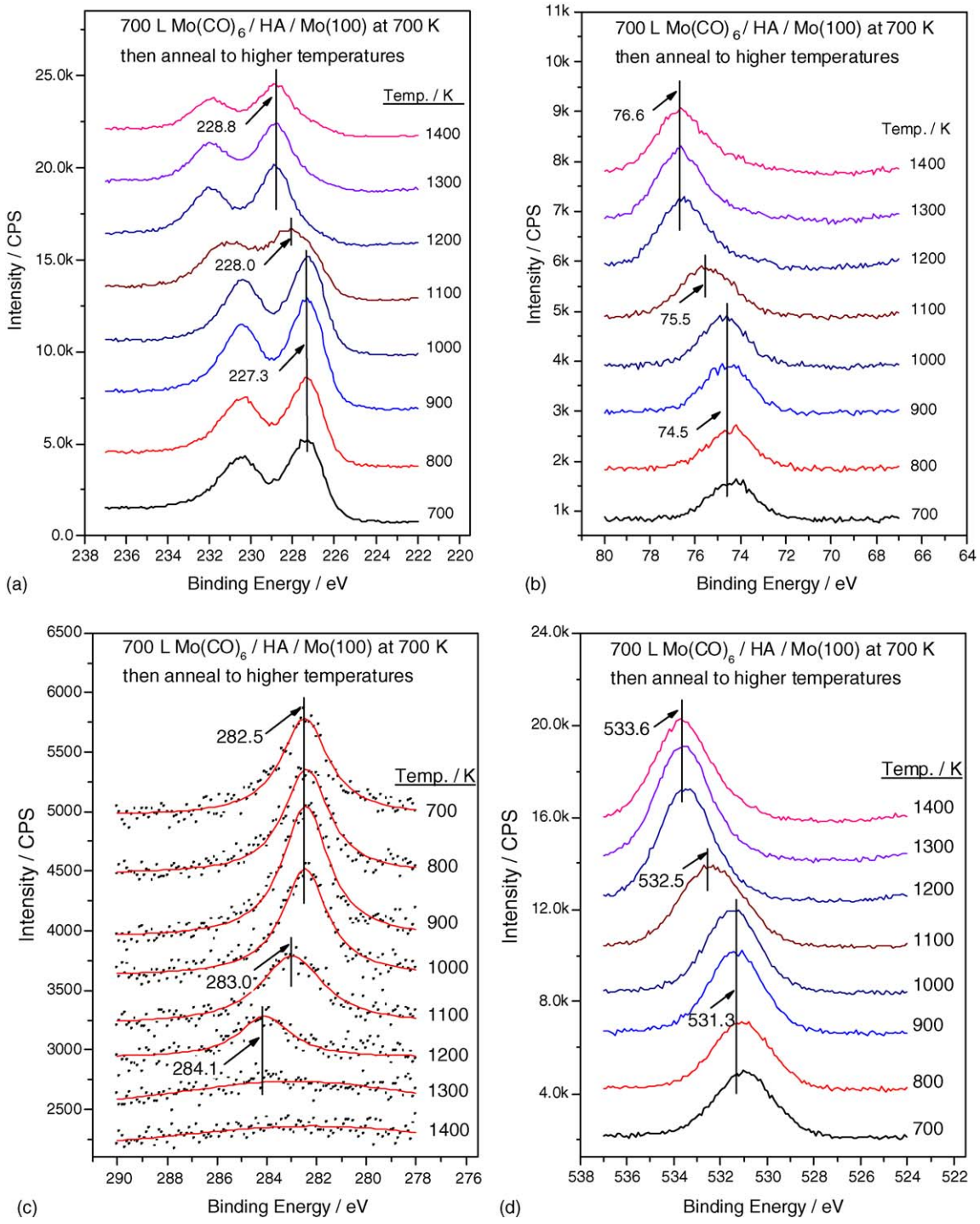

Fig. 7. Narrow scan Mg Kα X-ray photoelectron spectra of the (a) Mo 3d, (b) Al 2p, (c) C 1s and (d) O 1s regions following 700 L of $Mo(CO)_6$ deposited onto hydroxylated alumina at 700 K and heated to various temperatures, where annealing temperatures are displayed adjacent to the corresponding spectrum.

also from Fig. 6 that, for $Mo(CO)_6$ exposures below 100 L, the Mo 3d signal intensity increases almost linearly with exposure, but the binding energy does not vary. This suggests that more particles are formed on the surface with increasing $Mo(CO)_6$ exposure, while the particle sizes do not vary substantially. At high $Mo(CO)_6$ exposures, the uptake curve saturates suggesting that the molybdenum carbide coverage approaches a monolayer [39].

The data of Fig. 8 show that the reactive sticking probability of $Mo(CO)_6$ on hydroxylated alumina at 700 K is constant and approximately six times larger than that found for dehydroxylated alumina. This immediately implies this is due to the –OH groups on the HA surface. This is corroborated by the TPD data plotted in Fig. 4, where the H_2O desorption yield decreases with increasing $Mo(CO)_6$ exposure. The XPS data shown in Fig. 5 also suggest that hydroxyl groups are removed

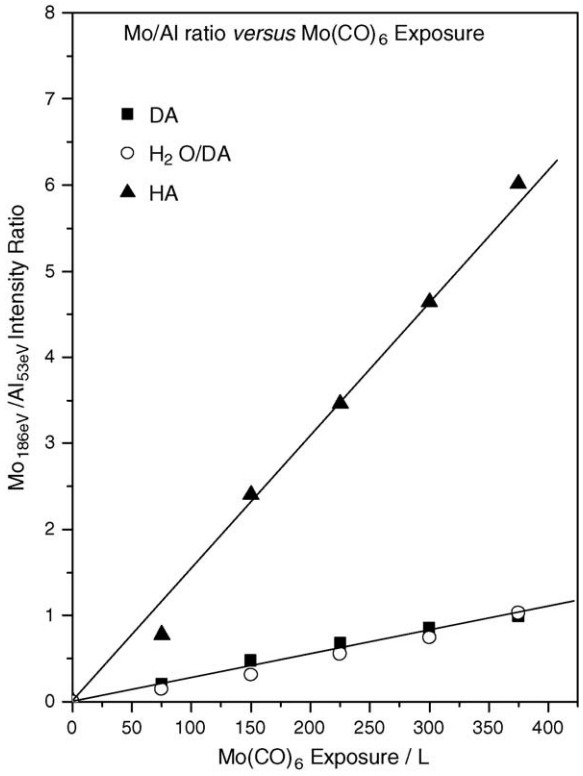

Fig. 8. Plot of the $Mo_{186\,eV}/Al_{53\,eV}$ peak-to-peak intensity ratio as a function of $Mo(CO)_6$ exposure at 700 K on hydroxylated alumina (▲), dehydroxylated alumina (■), and dehydroxylated alumina subsequently treated with water vapor (◯).

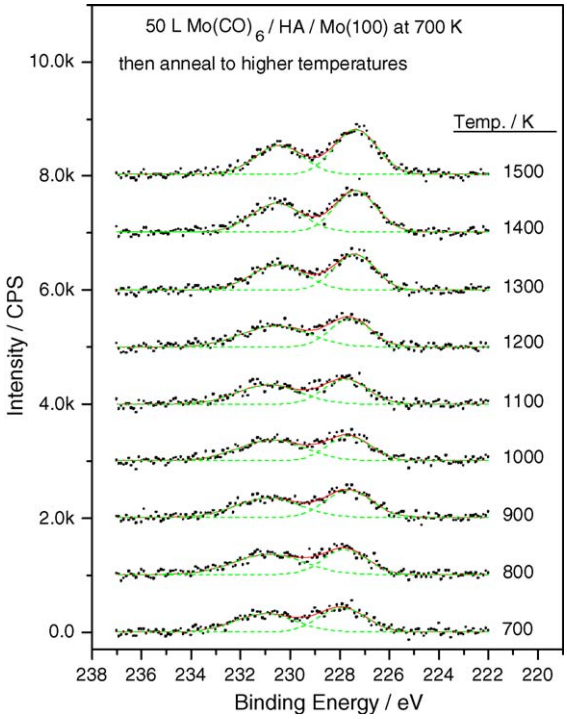

Fig. 9. Narrow scan Mg Kα X-ray photoelectron spectra of the Mo 3d region following 50 L of $Mo(CO)_6$ deposited onto hydroxylated alumina at 700 K and heated to various temperatures, where annealing temperatures are displayed adjacent to the corresponding spectrum.

by reaction with $Mo(CO)_6$, where it is found that O 1s binding energy becomes closer to that of dehydroxylated alumina following reaction with $Mo(CO)_6$. However, hydroxylating an initially dehydroxylated alumina surface does not increase the reaction probability (Fig. 8). It has been demonstrated previously that water reacts only with surface defect sites on α-Al_2O_3(0 0 0 1) at a water vapor pressure of $\sim 10^{-6}$ Torr [40], and that a threshold water pressure of ∼1 Torr is required to fully hydroxylate α-Al_2O_3(0 0 0 1) [41]. Although the alumina film formed here does not necessarily resemble a single crystal, it may still be that the hydroxylation conditions only form hydroxyl groups on existing surface defect sites without creating new ones so that, following hydroxylation of an initially dehydroxylated surface, no change in sticking probability is found (Fig. 8). Despite the differences in the $Mo(CO)_6$ reaction rate rates on DA and HA, identical carbides, both MoC and Mo_2C, are found on both alumina films (Fig. 3(a)). It is anticipated that, because of the –OH groups on HA, a larger concentration of molybdenum carbide islands will form on HA than on DA, but that the properties of each island are identical on both surfaces. Since ex situ AFM measurements (not shown) have revealed that the HA surface is rougher than the DA, this may be another reason that the reactive sticking probability of $Mo(CO)_6$ on HA is larger than on DA.

4.2. *Effect of annealing the film*

The loss of molybdenum is found for the thick, molybdenum-carbonyl-derived films (Figs. 1(b) and 7(a)) and ascribed to diffusion of molybdenum into the bulk of the sample. Such surface to bulk transport has been observed previously [42,43] where it was suggested that, on heating, some channels are formed in the alumina, allowing adsorbate diffusion to the bulk via these channels. This effect is not seen at low $Mo(CO)_6$ exposures (Fig. 9), presumably since the smaller molybdenum-containing particles are more strongly bound. Note that for molybdenum carbide films of various thicknesses formed on DA, no Mo diffusion to the bulk was found while annealing [22]. Since the diffusion is through channels developed during annealing, we expect that during the formation of dehydroxylated alumina (by repeated aluminum deposition–oxidation-annealing), these channels are blocked.

An increase in molybdenum binding energy is observed on heating to high temperatures (Fig. 7(a)) implying molybdenum oxidation. However, the data of Fig. 2(b) indicate that molybdenum is, in fact, reduced. It is may be that the diffused molybdenum is finely dispersed in the film causing an increase in binding energy [44]. Heating the sample to ∼1000 K causes an increase on the C/Mo ratio to form MoC due to carbon diffusion (Fig. 3(b)), and this effect has been observed previously [45].

TPD results (Fig. 4) reveal that CO desorbs in two states, both of which cause alumina reduction since metallic aluminum appears at 1100 K (Fig. 1(b)). It has been demonstrated that alumina reduction is due to the high-temperature reaction of carbidic carbon with alumina, verified using an alumina substrate formed using $H_2{}^{18}O$ [22]. Note, however, that the aluminum

formation temperature is 200 K lower on HA than on DA, presumably due to the larger amount of carbon deposited on HA (Fig. 5) than on DA [22].

Annealing the molybdenum carbide films formed on aluminum and DA to temperatures higher than 1300 K results in a Mo 3d binding energy lower than that of metallic Mo [22], which is assigned to the formation of an interfacial MoAl alloy. A similar situation is found here by depositing 50 L $Mo(CO)_6$ on HA and annealing to higher temperatures (Fig. 9), similarly assigned to a MoAl alloy. However, for thicker molybdenum carbide films, because of Mo diffusion into the bulk, this alloy formation is inhibited.

The overall reaction mechanism, following the above discussion, is presented in the following as

$$Mo(CO)_6 \xrightarrow{700\,K} Mo + 6CO \quad (1)$$

$$CO \xrightarrow{700\,K} C_{(ads)} + O_{(ads)} \quad (2)$$

$$CO + O_{(ads)} \xrightarrow{700\,K} CO_{2(g)} \quad (3)$$

$$Mo + C_{(ads)} \xrightarrow{700\,K} MoC_x \quad (4)$$

$$MoC_x + Al_2O_3 \xrightarrow{>800\,K} Mo + Al + CO_{(g)} \quad (5)$$

5. Conclusions

Molybdenum hexacarbonyl adsorbs on hydroxylated alumina at 700 K to form molybdenum carbides, where the stoichiometry is close to MoC at lower $Mo(CO)_6$ exposures, approaching Mo_2C as the exposure increases. The molybdenum is also slightly oxidized. The Mo $3d_{5/2}$ chemical shift suggests that small particles are formed at low $Mo(CO)_6$ exposures. At high $Mo(CO)_6$ exposures, the Mo $3d_{5/2}$ binding energy becomes identical to that of bulk molybdenum, suggesting the presence of large particles or the formation of a thin film. It is found that the carbonyl sticking probability at 700 K is about six times larger on hydroxylated alumina than on dehydroxylated alumina, an effect that is ascribed to the larger roughness of the hydroxylated alumina film, and the presence of surface defects created because of the removal of surface hydroxyl groups. Heating the surface carbide to high temperatures desorbs primarily CO and forms metallic aluminum. The loss of molybdenum from the surface at large $Mo(CO)_6$ exposures is ascribed to molybdenum diffusion into the alumina film. In this case, metallic aluminum and molybdenum segregate so that no alloy formation is found. At low $Mo(CO)_6$ exposures, both metallic aluminum and molybdenum remain at the surface so that a MoAl alloy is formed.

Acknowledgments

We gratefully acknowledge support of this work by the Chemistry Division of the National Science Foundation under grant number CTS-0105329.

References

[1] A. Brenner, J. Mol. Catal. 5 (1979) 157.
[2] E. Davie, D.A. Whan, C. Kemball, J. Catal. 24 (1972) 272.
[3] J. Smith, R.F. Howe, D.A. Whan, J. Catal. 34 (1974) 191.
[4] R. Thomas, J.A. Moulijn, J. Mol. Catal. 15 (1982) 157.
[5] A. Brenner, R.L. Burwell Jr., J. Am. Chem. Soc. 97 (1975) 2565.
[6] A. Brenner, R.L. Burwell Jr., J. Catal. 52 (1978) 353.
[7] R.F. Howe, Inorg. Chem. 15 (1976) 486.
[8] A. Kazusaka, R.F. Howe, J. Mol. Catal. 9 (1980) 183.
[9] K.P. Reddy, T.L. Brown, J. Am. Chem. Soc. 117 (1995) 2845.
[10] A. Zecchina, E.E. Platero, C.O. Areán, Inorg. Chem. 27 (1988) 102.
[11] R.F. Howe, I.R. Leith, J. Chem. Soc, Faraday Trans. I 69 (1973) 1967.
[12] W.M. Shirley, B.R. McGarvey, B. Maiti, A. Brenner, A. Cichowlas, J. Mol. Catal. 29 (1985) 259.
[13] M. Kaltchev, W.T. Tysoe, J. Catal. 193 (2000) 29.
[14] M. Kaltchev, W.T. Tysoe, J. Catal. 196 (2000) 40.
[15] Y. Wang, F. Gao, M. Kaltchev, D. Stacchiola, W.T. Tysoe, Catal. Lett. 91 (2003) 83.
[16] Y. Wang, F. Gao, M. Kaltchev, W.T. Tysoe, J. Mol. Catal. A: Chem. 209 (2004) 135.
[17] Z. Jiang, W. Huang, J. Jiao, H. Zhao, D. Tan, R. Zhai, X. Bao, Appl. Surf. Sci. 229 (2004) 43.
[18] C.C. Williams, J.G. Ekerdt, J. Phys. Chem. 97 (1993) 6843.
[19] L. Rodrigo, K. Marcinkowska, P.C. Roberge, S. Kaliaguine, J. Catal. 107 (1987) 8.
[20] I.V. Elav, B.N. Shelimov, V.B. Kazansky, J. Catal. 113 (1988) 256.
[21] Y. Wang, F. Gao, W.T. Tysoe, J. Mol. Catal. A: Chem. 236 (2005) 18.
[22] Y. Wang, F. Gao, W.T. Tysoe, J. Mol. Catal. A: Chem. 235 (2005) 173.
[23] M.G. Kaltchev, A. Thompson, W.T. Tysoe, Surf. Sci. 391 (1997) 145.
[24] W.J. Wytenburg, R.M. Lambert, J. Vac. Sci. Technol. A 10 (1992) 3597.
[25] P.J. Chen, M.L. Colaianni, J.T. Yates Jr., Phys. Rev. B 41 (1990) 8025.
[26] C. Zhang, M.A. Van Hove, G.A. Somorjai, Surf. Sci. 149 (1985) 326.
[27] A. Wolowik, M. Janik-Czachor, Mater. Sci. Eng. A 267 (1999) 301.
[28] D. Briggs, J.T. Grant (Eds.), Surface Analysis by Auger and X-ray Photoelectron Spectroscopy, IM Publications and Surface Spectra Limited, UK, 2003.
[29] D.L. Cocke, E.D. Johnson, R.P. Merrill, Catal. Rev. Sci. Eng. 26 (1984) 163.
[30] Th. Dittrich, H.-J. Muffler, M. Vogel, T. Guminskaya, A. Ogacho, A. Belaidi, E. Strub, W. Bohne, J. Rohrich, O. Hilt, M.Ch. Lux-Steiner, Appl. Surf. Sci. 240 (2005) 236.
[31] K. Edamoto, M. Sugihara, K. Ozawa, S. Otani, Surf. Sci. 561 (2004) 101.
[32] J.A. Rodriguez, J. Dvorak, T. Jirsak, J. Phys. Chem. B 104 (2000) 11515.
[33] J.M. Horn, Z. Song, D.V. Potapenko, J. Hrbek, M.C. White, J. Phys. Chem. B 109 (2005) 44.
[34] T. Schoreder, J. Zegenhagen, N. Magg, B. Immaraporn, H.-J. Freund, Surf. Sci. 552 (2004) 85.
[35] H.H. Hwu, J.G. Chen, Chem. Rev. 105 (2005) 185.
[36] P. Legare, Y. Sakisaka, C.F. Brucker, T.N. Rhodin, Surf. Sci. 139 (1984) 316.
[37] V. Murgai, S. Raaen, M. Strongin, R.F. Garrett, Phys. Rev. B 33 (1986) 4345.
[38] G.K. Wertheim, S.B. DiCenzo, S.E. Youngquist, Phys. Rev. Lett. 51 (1983) 2310.
[39] G.K. Wertheim, S.B. DiCenzo, Phys. Rev. B 37 (1988) 844.
[40] V. Coustet, J. Jupille, Surf. Sci. 307–309 (1994) 1161.
[41] P. Liu, T. Kendelewicz, G.E. Brown Jr., E.J. Nelson, S.A. Chambers, Surf. Sci. 417 (1998) 53.
[42] J.G. Chen, J.E. Crowell, J.T. Yates Jr., Surf. Sci. 185 (1987) 373.
[43] M. Heemeier, S. Stempel, Sh.K. Shaikhutdinov, J. Libuda, M. Banmer, R.J. Oldman, S.D. Jackson, H.-J. Freund, Surf. Sci. 523 (2003) 103.
[44] C.R. Henry, Surf. Sci. Rep. 31 (1998) 231.
[45] T.P. St. Clair, S.T. Oyama, D.F. Cox, S. Otani, Y. Ishizawa, R.-L. Lo, K. Fukui, Y. Iwasawa, Surf. Sci. 426 (1999) 187.